CHAPTER 4

RESULTS AND DISCUSSION

Chapter 4

Results – Material Characterization

4.1 General Appearance

The lead sulphide synthesized appears as a greyish black powder. This is shown in Figure 4.1.

Figure 4.1. A photograph of PbS powder.

The tin sulphide prepared in this work was deposited as brownish black powder. Figure 4.2 shows a photograph of powdered SnS.

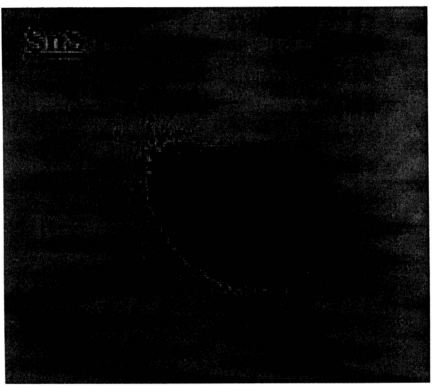

Figure 4.2. A photograph of SnS powder.

In this work two samples of sulphide based anodes namely PbS and SnS were prepared. A chemical bath deposition technique was selected as the method for preparing PbS because it is simple and inexpensive. More over

this technique does not require high voltages, high currents nor high temperatures.

The steps involved in the reaction mechanism for PbS deposition can be treated on similar lines to the description for $Cd_xPb_{1-x}S$ films (Upadhaya and Chandra, 1994) where the overall reaction giving PbS can be simply written as

$$Pb^{2+} + S^{2-} \longrightarrow PbS$$

In this preparation, the ammonium hydroxide solution were added drop by drop to ensure the OH^- ion react with the HS^- produced from the thiourea. The formation of PbS is shown by the precipitation of the greyish black precipitate. This was later confirmed by x-ray diffraction experiments. In the case of SnS, the double decomposition method was employed. In this preparation, it is important that Sn^{2+} is always present and not Sn^{4+} since Sn^{2+} is a reducing agent. The insoluble sulphide formed in the reaction can be separated from the acid by filtration.

$$H_2S\,(g) + Sn\,SO_4\,(aq) \longrightarrow Sn\,S\,(s) + H_2\,SO_4\,(aq)$$

Since acid is also formed in the reaction, only the most insoluble sulphide will be precipitated. The presence of acid retards the ionisation of the hydrogen sulphide and pushes the equilibrium to the left and therefore the concentration of S^{2-} is low.

$$H_2S\ (g) \rightleftharpoons 2H^+\ (aq) + S^{2-}\ (aq)$$

In alkaline solutions however the less insoluble sulphides will be precipitated since the equilibrium is shifted to the right, giving a higher S^{2-} ion concentration (Brown, 1986).

4.2 X-ray Diffraction (XRD)

Figure 4.3 shows the X-ray diffractogram of PbS, thiourea, $[(NH_2)_2\ CS]$ and lead nitrate$[Pb(NO_3)_2]$. Sharp and intense diffraction lines occur at 2θ = 30.0°, 25.8° and 42.9° indicating the crystalline nature of PbS. The 2θ angle for PbS was taken from 20° onwards since the JCPDS data shows no peaks with 2θ angle below 20°.

The d spacing ($\overset{0}{A}$) values and the 2θ values observed from the X-ray diffractogram are compared with the 2θ values and d spacing ($\overset{0}{A}$) values obtained from the Powder Diffraction File (1995), JCPDS 5-592, PDF-2 Database Sets 1 – 45. The diffraction angles (2θ) of the samples and the corresponding d values are given in Table 4.1

Table 4.1 Diffraction angle (2θ) and d spacing ($\overset{0}{A}$) of PbS compared with JCPDS data.

Sample	Observed values			JCPDS		
	2θ (°)	d-spacing ($\overset{0}{A}$)	Intensity (%)	2θ (°)	d-spacing ($\overset{0}{A}$)	Intensity (%)
PbS	30.0	2.976	100	30.1	2.969	100
	25.8	3.451	80	26.0	3.429	84
	43.0	2.104	60	43.1	2.107	57
	50.8	1.791	38	51.0	1.790	35
	52.4	1.740	15	53	1.714	16

The diffraction angle and d spacing of the synthesized PbS is quite close with the JCPDS reference. The diffractograms of the starting materials i.e. thiourea and $Pb(NO_3)_2$ do not show any similarity with that of PbS. Due to this the sample is assigned to PbS.

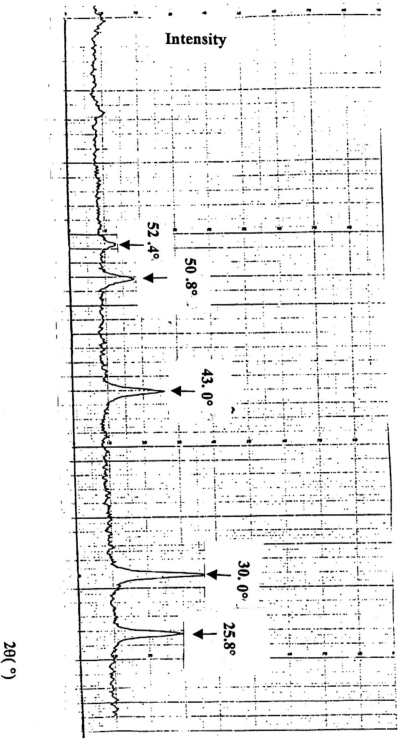

Figure 4.3 (a). X-ray diffractogram of lead sulphide, PbS

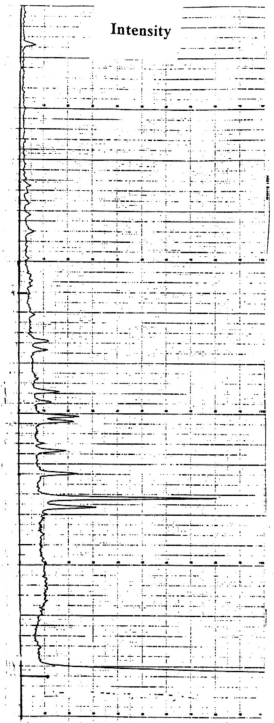

Figure 4.3 (b). X-ray diffractogram of thiourea

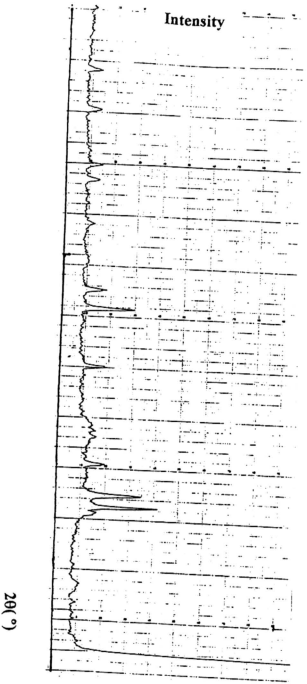

Figure 4.3 (c). X-ray diffractogram of lead nitrate

The X-ray diffractogram of the prepared SnS (Figure 4.4) and the 2θ angles are quite close with the available references JCPDS file 32-1361 (alpha SnS), JCPDS file 34-1439 (SnS), JCPDS file 39-354 (SnS, Herzenbergite) since there are three JCPDS patterns for SnS (Table 4.2).

Table 4.2. Diffraction angles and d spacing values of SnS compared with JCPDS data

Sample	**Observed**		**JCPDS 32-1361**		**JCPDS 34-1439**		**JCPDS 39-354**	
	2θ (°)	Intensity (%)	2θ (°)	Intensity (%)	2θ (°)	Intensity (%)	2θ (°)	Intensity (%)
SnS	31.5	100	31.4	100			31.5	100
	63.2	100			64.7	100		
	38.9	38	38.9	40				
	26.0	46					26.0	50

The X-ray diffractogram of the prepared sample was compared with three JCPDS patterns as was also done by the ISITEM group from Laboratoire de Genie des Materiaux, Nantes Cedex, France who prepared SnS_2. In that work they have compared their SnS_2 sample with two JCPDS pattern of SnS_2 i.e. JCPDS file 40-1466 and JCPDS file 4-0-1467. In our work the peaks at 2θ=31.5° and 63.2° from the X-ray diffractogram of the sample matches well with all the JCPDS pattern. Due to this the X-ray

diffractogram in Figure 4.4(a) is assigned to SnS. Figure 4.4(b) shows the X-ray diffractogram of $SnSO_4$. Upon comparing PbS and SnS X-ray diffractograms PbS has a more crystalline nature than SnS since the peaks in PbS are sharper.

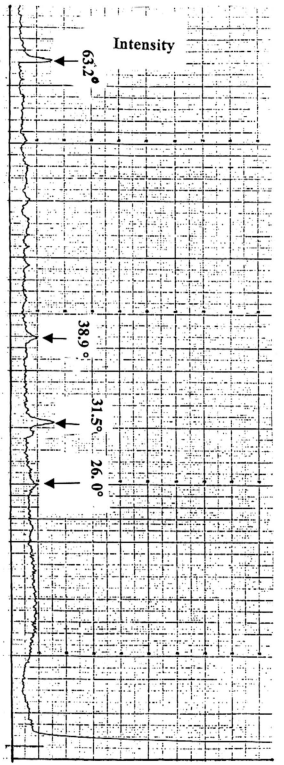

Figure 4.4 (a). X-ray diffractogram of SnS.

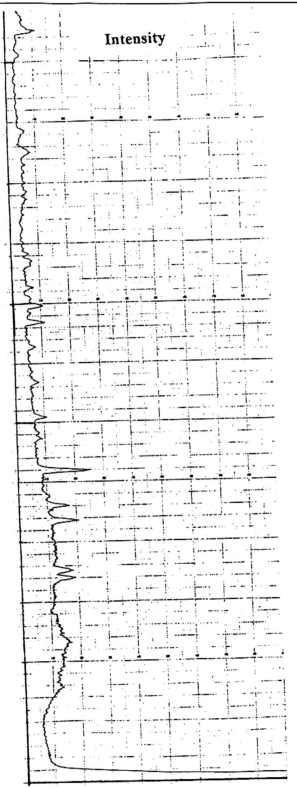

Figure 4.4 (b). X-ray diffractogram of $SnSO_4$

4.3 Energy dispersive Analysis of X-rays (EDAX)

Figure 4.5 shows the EDAX spectrum for PbS. Peaks attributable to lead and sulphur are clearly shown. The elemental composition percentages taken at four different spots gave lead to sulphur ratio of 48%:52% (Table 4.3). Therefore it can be concluded that the product of the chemical bath deposition is PbS within the systematic error of the equipment.

Table 4.3. Elemental composition percentage of PbS

Sample	Element	% composition		% error
		EDAX	Expected	
PbS	Pb	48	50	± 4.0
	S	52	50	

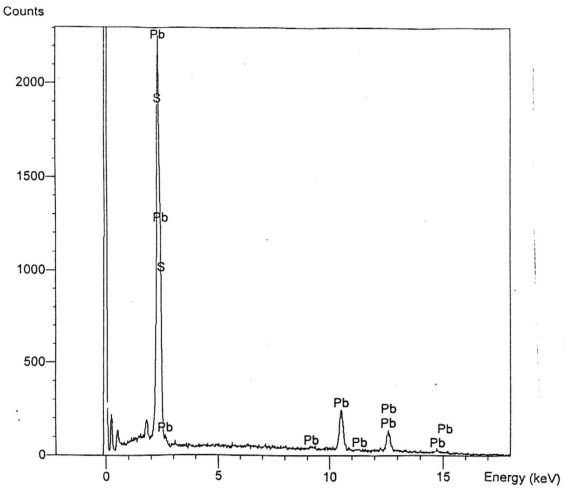

Figure 4.5. EDAX spectrum for PbS

The EDAX spectrum of the SnS shows the peaks for sulphur and tin. The average of the elemental percentage composition at four spots (Table 4.4) are in agreement with the tin and sulphur ratio in the formula SnS.

Table 4.4. Elemental composition percentage of SnS

Sample	**Element**	**% composition**		**% error**
		EDAX	**Expected**	
SnS	Sn	50.02	50	± 0.04
	S	49.98	50	

By examining Table 4.4 , the ratio of Sn : S in the prepared sample can be derived to be 1: 1.

The EDAX spectrum in Figure 4.6 shows the peaks attributable to Sn and S.The quantitative analysis in Table 4.3 shows that the ratio of Sn:S is 1:1.

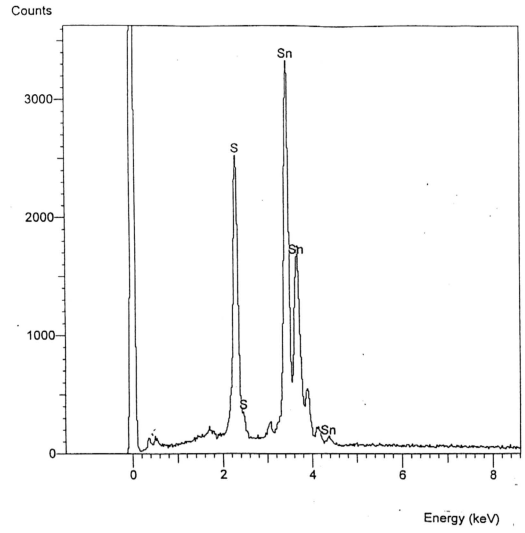

Figure 4.6. EDAX spectrum for SnS

4.4 Scanning electron Microscopy (SEM)

Figure 4.7 shows the SEM micrograph of PbS. At 1.75K magnification it is needle like and highly crystalline in nature. The SEM micrograph shows even and smooth distribution of particles.

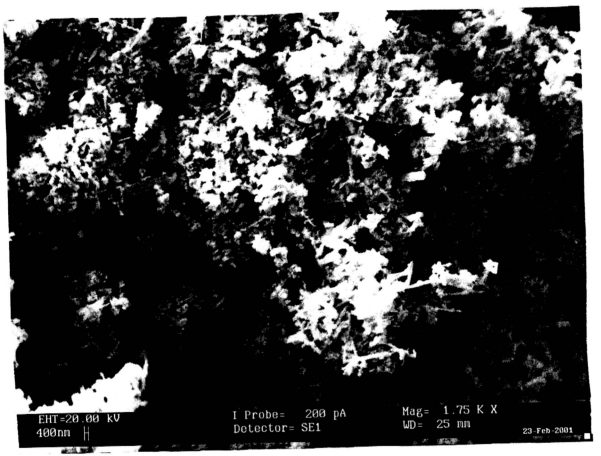

Figure 4.7. SEM micrograph of PbS

(1.75 K magnification)

The surface morphology of the samples were studied using scanning electron microscopy. The nature and the morphology of a sample is an important property for both electrolyte and electrode (Jacob, 1999). The SEM micrographs shows that the PbS sample has needle like structure which is more crystalline than SnS. The less define crystalline structure in SnS suggests that it is more amorphous and this is confirmed by its X-ray diffractogram. The crystalline nature of PbS has been observed in the X-ray diffractogram analysis .

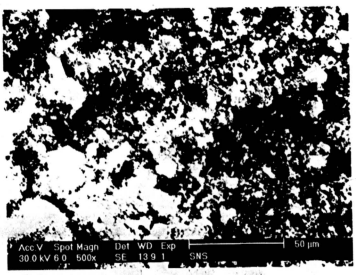

Figure 4.8 SEM micrograph of SnS at 500x magnification

At 500x magnification the micrograph of SnS shows worm like structures or fibrils which are almost evenly distributed. The presence of the fibrils along with dark region suggests that there is some degree of amorphocity in the sample i.e. it is less crystalline in nature than PbS. The particles appear to be smooth.The fibrils structure is still seen and more evenly distributed observed at a higher magnification of 1.76 K (Figure 4.9). The area of the dark regions is reduced. Particles seemed to be smoother without obvious edges.

Figure 4.9. SEM micrograph of SnS at higher magnification (1.76 K).

The SEM micrograph of SnS is similar to the SEM micrograph of SnO_2 (Figure 4.10) where the particles tend to exhibit a uniform distribution in terms of particle shape size and texture (Morales and Sanchez, 1999).

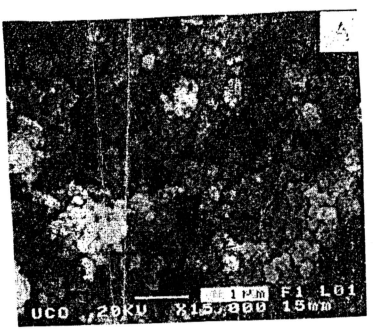

Figure 4.10. SEM micrograph of SnO_2 (Morales and Sanchez, 1999)

Both micrographs of PbS and SnS show that most of the particles are dispersed on the surface uniformly and PbS is more crystalline in nature than SnS.

4.5 Impedance Spectroscopy

The conductivity of PbS and SnS were measured at room temperature (22°C) and at 90°C. Each measurement was repeated twice.

A representative of the complex impedance plots for PbS is exhibited in figures 4.11 and 4.12 and the values of the bulk resistance obtained from the complex impedance is tabulated in Table 4.5

Table 4.5. Bulk resistance and conductivity values for PbS at room temperature and at 90°C. Area of contact = 2.405 cm^2

Temperature	Sample PbS	Thickness l(cm)	Bulk resistance R_b (Ω)	Conductivity σ (S cm^{-1})	Average conductivity σ (S cm^{-1})
Room temperature	S1	0.080	1.3×10^2	2.5×10^{-4}	2.6×10^{-4}
	S2	0.082	1.2×10^2	2.7×10^{-4}	
90°C	S1	0.038	44.00	3.3×10^{-4}	3.3×10^{-4}
	S2	0.035	44.00	3.3×10^{-4}	

From Table 4.5, it can be concluded that the average conductivity of PbS are as follows

at RT , $\sigma = 2.6 \times 10^{-4}$ S cm^{-1}

at 90°C , $\sigma = 3.3 \times 10^{-4}$ S cm^{-1}

Hence , σ does not increase much at 90°C.

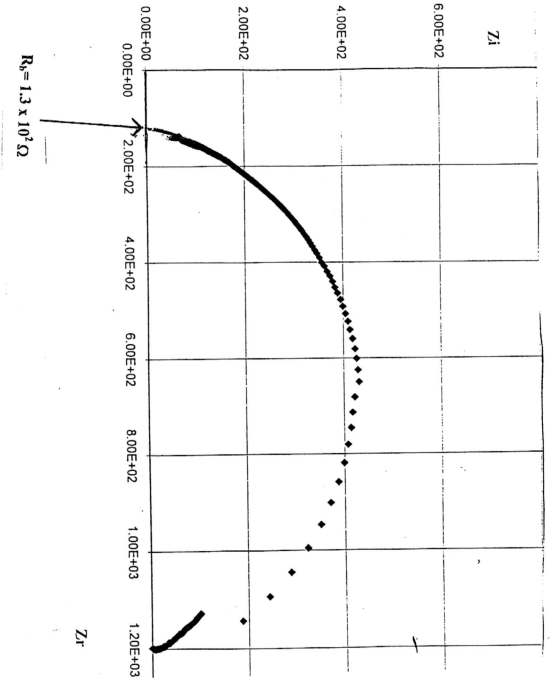

Figure 4.11. A representative of Impedance plot for PbS at room temperature

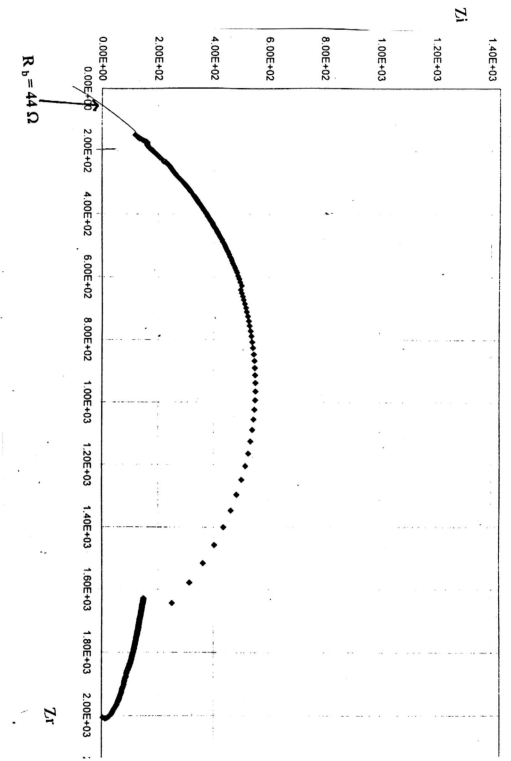

Figure 4.12. A representative of Impedance plot for PbS at 90°C.

Figures 4.13 and 4.14 show the impedance plots of the tested SnS samples. The bulk resistance, R_b determined from the impedance plots and conductivity values, σ, for SnS at room temperature and 90°C are listed in Table 4.6

Table 4.6. Bulk resistance and conductivity of SnS at RT and 90°C Area of contact = 2.405cm^2

Temperature	Sample SnS	Thickness l (cm)	Bulk Resistance Rb (Ω)	Conductivity σ (S cm^{-1})	Average conductivity σ (S cm^{-1})
RT	S1	0.080	4.2×10^4	7.9×10^{-7}	5.3×10^{-7}
	S2	0.084	3.6×10^4	2.7×10^{-7}	
90°C	S1	0.030	7.0×10^3	1.8×10^{-6}	2.9×10^{-6}
	S2	0.032	3.3×10^3	4.1×10^{-6}	

The following average conductivities of SnS can be drawn from Table 4.6

at RT , $\sigma = 5.3 \times 10^{-7}$ S cm^{-1}

at 90°C , $\sigma = 2.9 \times 10^{-6}$ S cm^{-1}

Hence for SnS σ increases at higher temperature.

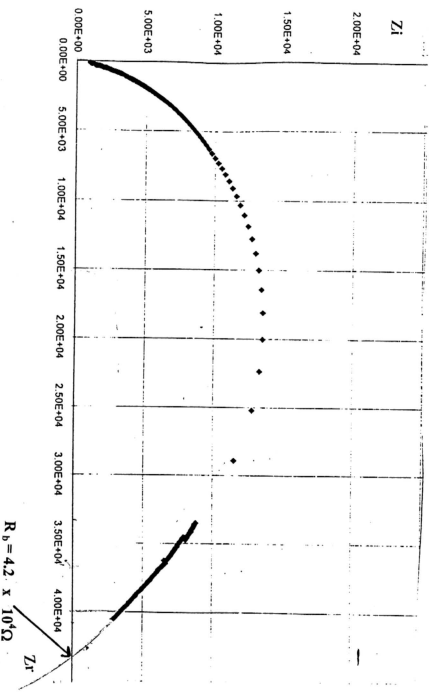

Figure 4.13. Impedance plot for SnS at room temperature.

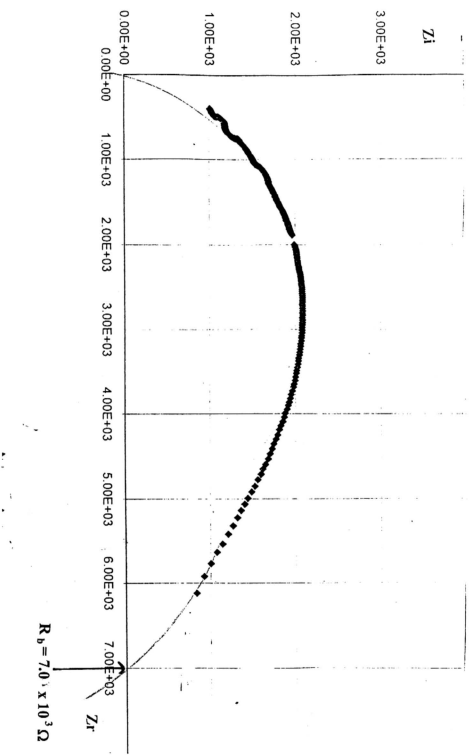

Figure 4.14. Impedance plot for SnS at 90°C

PbS and SnS are semiconductor materials and one of their most important properties is electrical conductivity. For a material to be used as anode, it must have high electrical conductivity values (Megahead and Ebner, 1995) . The important electrical parameters of semiconductors besides conductivity are resistivity, mobility and carrier life time (Sze, 1985).

- **Electrical Conductivity At Room Temperature**

From the impedance plots, the conductivities of PbS and SnS were found to be

PbS : $\sigma = 2.6 \times 10^{-4}$ Scm^{-1}

SnS : $\sigma = 5.3 \times 10^{-7}$ Scm^{-1}

It can be seen that the conductivity of PbS is higher than the conductivity of SnS by more than 100 times at room temperature.

- **Electrical Conductivity at 90°C**

The results obtained from tables 4.5 and 4.6 show that σ, the conductivity values increases at 90°C.

Table 4.7. Comparison of conductivity values between PbS and SnS at 90°C.

Sample	σ (S cm^{-1})	
	Room temperature	90°C
PbS	2.6×10^{-4}	3.3×10^{-4}
SnS	5.3×10^{-7}	2.9×10^{-6}

Both PbS and SnS are semiconductor materials and the conducting species are electrons. Therefore at higher temperatures the mobility of the electrons increases and thus increasing the conductivity. Mobility is an important parameter since it describes how strongly the motion of an electrons is influenced by as applied electric field (Sze, 1985).

Electrical conductivity in semiconductor is small due to lack of free electrons. Electrical conductivity, $\sigma = \eta e \mu$ where ηe is the amount of electrons and μ is the mobility of electrons. Conductivity is also structurally dependent, the insignificant change in σ, after raising the temperature to 90° C could imply that the structure of PbS is stable that conductivity is not enhanced.

The electrical conductivity values (at RT) for PbS and SnS obtained in this work is expected since the values is within the range of conductivities for semiconductors (Sze, 1985). The range of conductivities for insulators, semiconductors and conductors are shown in Figure 4.15.

Unfortunately, complex impedance plots for PbS and SnS obtained from impedance spectroscopy are very rare in the literature and no further comparison is possible to be made between the results of this work and those already published.

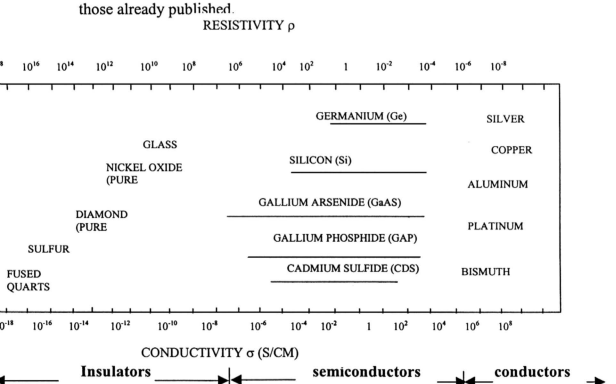

Figure 4.15. Range of conductivities for insulators, semiconductors and conductors (Sze, 1985)

4.6 Cyclic Voltammetry

Cyclic voltammetry of PbS

The Pb^{II}/ Pb have a potential -0.13V (Lide, 1990) relative to hydrogen electrode $2H^+/H_2$. From Figure 4.16 a reversible wave at around 3.0 V versus Li^+/ Li electrode at scan rate 100 mV s^{-1} conforms to the above reversible redox reaction. The presence of reversible peaks shows that lithium ion has undergone intercalation and deintercalation processes.

At 400 mV s^{-1} scan rate the currents remained the same thus indicating that the reaction is not a diffusion control reaction (Figure 4.17).

The presence of this reversible peak can be assigned to the redox reaction

$$PbS + Li \rightleftharpoons Pb + Li_2S$$

It can be elaborated as

$$Pb^{II} + 2e \rightleftharpoons Pb \; ; \qquad \text{electron transfer control}$$

$$2Li^+ + Pb \rightleftharpoons 2Li + Pb^{II}$$

This reversible reaction is consistent with the XRD pattern (Figure 4.16) in

which PbS peaks appeared after cyclic voltammetry experiments. The results above show that the cell was able to undergo redox reaction and the insertion and deinsertion of lithium ions are reversible and hence the ability of PbS as anode.

In the X-ray diffractogram (Figure 4.18) of the electrode after the cyclic voltammetry experiments, the peak intensity of the PbS starting material present decreases assuming not all Pb is oxidized to PbS. The original peaks do not entirely disappear and it is believe that not all of the starting material has been consumed.

There are other reversible peaks appearing at different potentials probably due to the different environment experienced by the electrochemical reactions. These redox couples can be explained if the Pb formed react reversibly with lithium ion to form the LiPb alloy or LiPbS alloy .

Some possible mechanisms are

$$Pb^{II} + 2Li^{+} + 2e \longrightarrow LiPb$$

$$xPb^{II} + yLi^{+} + ye \longrightarrow Li_y(Pb)_x$$

$$yPbS + xLi \longrightarrow Li_x(PbS)_y$$

Zhong et al (2000) during their work of barium metaplumbate , (a two phase compound of composition $BaPbO_3$ and PbO) an anode material with perovskite structure, suggested the following mechanism for PbO. Firstly is the reduction of PbO in the compound i.e.

$$Pb^{2+} + 2e \longrightarrow Pb$$

Secondly the remaining PbO react with Li during the electrochemical oxidation and reduction to form a new compound, possibly a Pb-Li alloy i.e.

$$PbO + xLi \longrightarrow Li_xPb + Li_2O$$

This is an irreversible reaction according to Zhong et al (2000). These led to the question whether other tin and lead compounds i.e. SnS and PbS could be used as anode in lithium rechargeable batteries and have similar mechanism.

However the studies of the different phases of alloy formed is beyond the scope of the studies of this work.

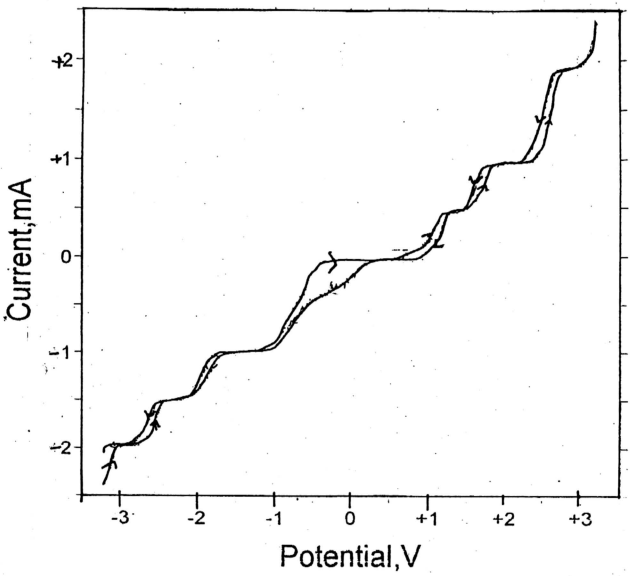

Figure 4.16. Cyclic voltammogram of PbS at 100 mV s^{-1} scan rate at room temperature. Both reference and counter electrode are lithium foil. The electrolyte is $LiCF_3SO_3$ (1M)/EC/DMC

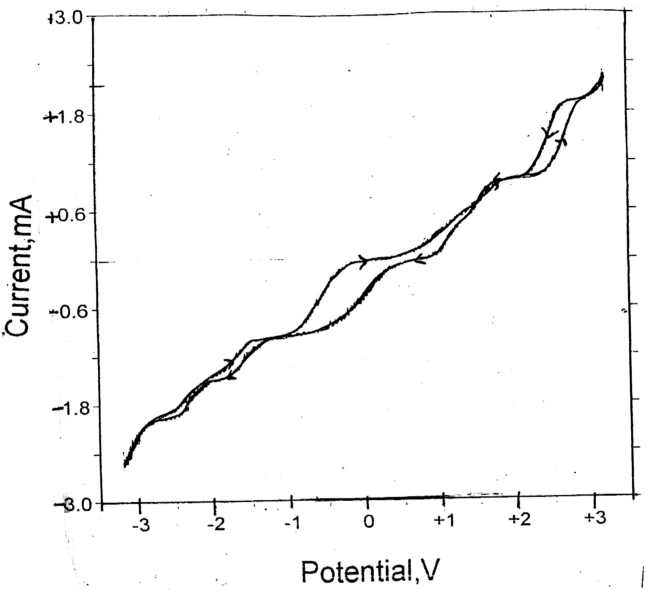

Figure 4.17. Cyclic voltammogram of PbS at 400mV s^{-1} scan rate at room temperature. Both reference and counter electrode are lithium foil. The electrolyte is $LiCF_3SO_3$ (1M)/EC/DMC

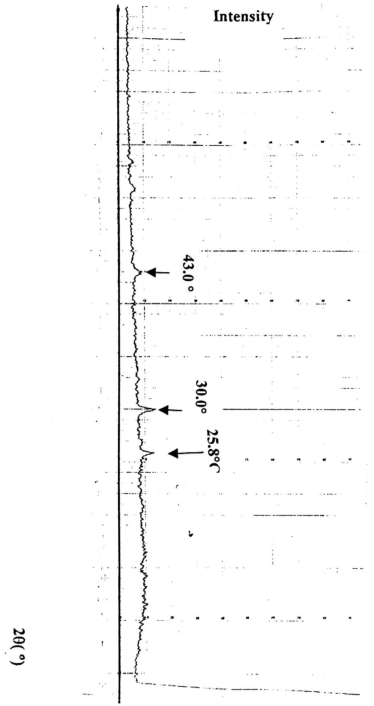

Figure 4.18. X-ray diffractogram for PbS electrode after cyclic voltammetry experiments.

Cyclic voltammetry of SnS

A cyclic voltammogram of a SnS sample with 400 mVs^{-1} scan rate is shown in Figure 4.19. A broad wave is seen, indicating many redox loops overlapping one another and that the reaction is electron transfer control. Since the 400 mVs^{-1} scan rate cyclic voltammogram were not clearly seen, so the cyclic voltammogram with 100 mV s^{-1} (Figure 4.20) was used for analysis. A reduction peak was observed around 1.0 V. To analyse the cyclic voltammogram even better, the cyclic voltammogram with 50 mV s^{-1} scan rate was studied which is shown in figure 4.21. A similar reduction peak at around 1.0 V vsersus Li^{+}/Li was observed by Momma et al (2000) while studying the SnS_2 material as a potential anode which they assigned to the formation of Sn metal from the SnS_2 powder. This reduction peak is thought to be attributed to the reduction

$$Sn^{II} + 2e \longrightarrow Sn$$

In order to confirm the formation of Sn, XRD experiments were carried out. Figure 4.22 shows the XRD pattern after cyclic voltammetry experiments. An examination of the XRD pattern shows that all SnS peak

disappeared after cycling except for peak at $2\theta = 31^{\circ}$ which is thought to be the tin peak since this peak agree with the JCPDS pattern of tin and a maximum peak at $2\theta = 26^{\circ}$ was observed. From this observation it is assumed that all of the SnS has been used up in the formation of tin particles.

Many research has been carried out to improved cycleability and increased capacity for lithium intercalation. Recent developments suggest that alloy systems can be made to work well as anodes for Li - ion cell. For example, in 1994 Fuji Photo Film Co. Ltd filed a patent for rechargeable lithium batteries in which amorphous tin based composite oxide and not carbon were used as anode materials (Hong Li et al., 1999). Idota et al (1994) claimed that the mechanism involved in the reversible reaction of lithium with the anode (tin as well as other group IV, oxides and oxide composite glasses) is or of intercalation, and that the process does not involve the formation of tin. However according to Courtney and Dahn (1997) the compounds described by Idota et al (1994) react with about 4 - 7 Li atoms per tin atom, which is much larger than that normally observed for intercalation systems. A reversible range of one or two lithium atoms per metal is more typical. Thus this mechanism seemed unlikely to Courtney and Dahn (1997) and they investigated the four compounds SnO, SnO_2,

Li_2SnO_3 and $SnSiO_3$ glass as representative to those studied by Idota et al (1994). Courtney and Dahn (1997) suggested a two steps reaction mechanism for the reaction of lithium with oxides based on tin element. Initially a decomposition reaction takes place that yields Li_2O and Sn as represented by the following reaction

$$SnO_2 + 4Li \longrightarrow Sn + 2Li_2O \quad (1)$$

$$mSn + nLi \longleftrightarrow Li_nSn_m \quad (2)$$

$$(LiSn, Li_7Sn_3, Li_5Sn_2, Li_{13}Sn_5, Li_7Sn_2, Li_{22}Sn_5)$$

It was also reported that Liu et al (1998) has studied electrode reaction of SnO_2 with lithium and their Raman spectra results have confirmed the two steps reaction mechanism.

Unlike PbS, the SnS reduction reaction is an irreversible process and the reduction peak is broader for SnS than PbS. The formation of tin is confirmed by the existing of the peak at $2\theta = 30.2\ ^{\circ}$. The declining of the peak confirm that the SnS loses its sulphur leaving regions of tin metal.

The other reversible peaks are assigned to the reversible formation and decomposition of LiSn alloy i.e. the alloying /dealloying of lithium with

tin. These phases are probably due to the formation of LiSn, Li_7Sn_3, Li_5Sn_2, $Li_{13}Sn_5$, $Li_{22}Sn_5$ alloy as suggested by Courtney and Dahn (1997).

The simplest alloy formation is thought to be

$$Sn^{II} + 2Li \rightarrow Li_2Sn$$

Since the peak at $2\theta = 26^{\circ}$ is the maximum peak and cannot be assigned to Li peak ($2\theta = 42.3^{\circ}$) or S peak ($2\theta = 23.08^{\circ}$) this peak might be due to the alloy peak whose data is not found in JCPDS. The studies of the alloy formation is again beyond the scope of this work and further study of the system is required for a more detailed explanation of the insertion and deinsertion mechanism.

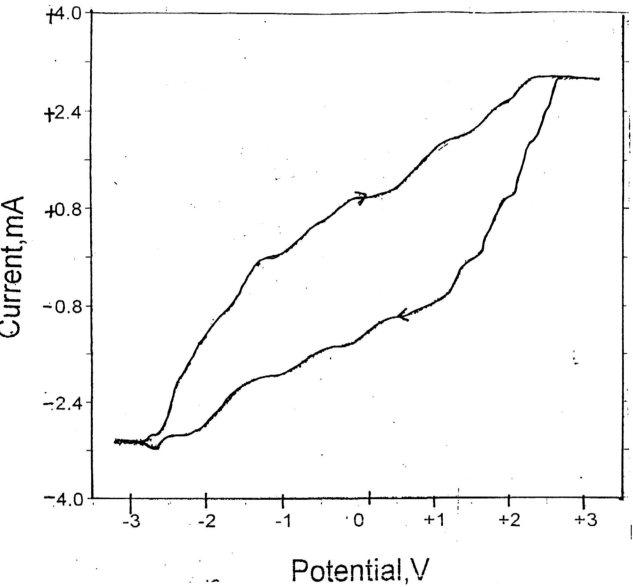

Figure 4.19. Cyclic voltammogram of SnS at 400mVs $^{-1}$ scan rate at room temperature. Both reference and counter electrode are lithium foil. The electrolyte is $LiCF_3SO_3$ (1M)/EC/DMC

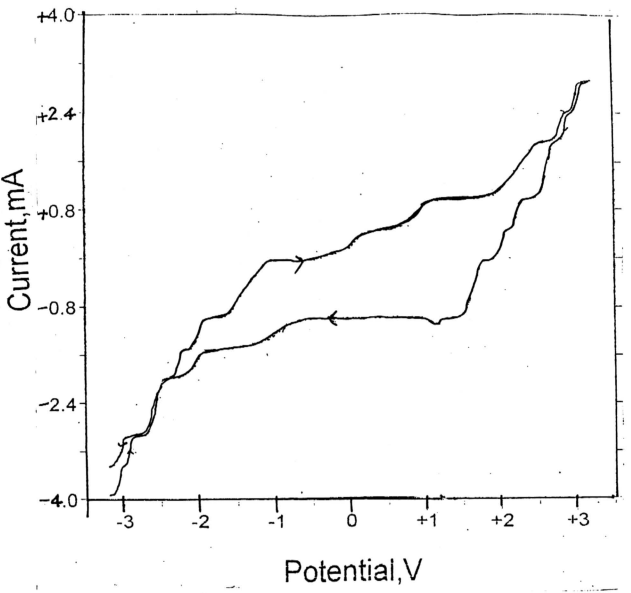

Figure 4.20. Cyclic voltammogram of SnS at 100mVs $^{-1}$ scan rate at room temperature. Both reference and counter electrode are lithium foil. The electrolyte is $LiCF_3SO_3$ (1M)/EC/DMC

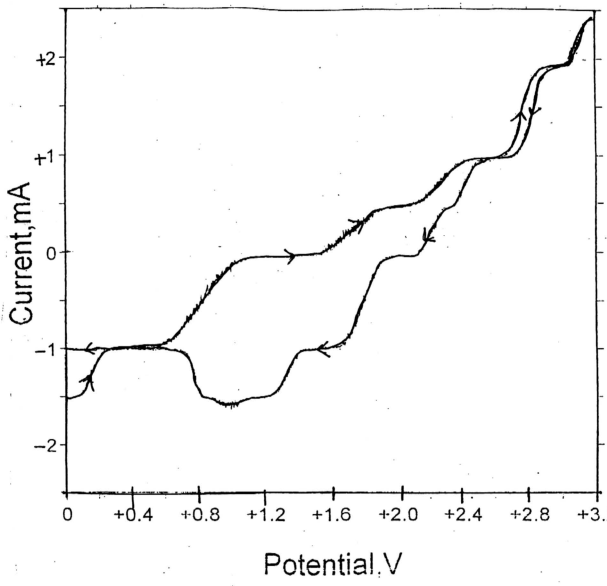

Figure 4.21. Cyclic voltammogram of SnS at 50mVs $^{-1}$ scan rate at room temperature. Both reference and counter electrode are lithium foil. The electrolyte is $LiCF_3SO_3$ (1M)/EC/DMC

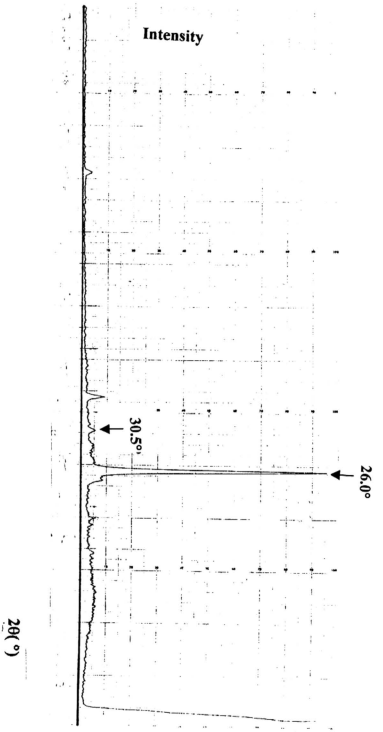

Figure 4.22. X- ray diffractogram of SnS after cyclic voltammetry experiments.

4.7 Battery Characterisation

4.7.1 Battery Fabrication

The conductivities of PbS and SnS used for the battery fabrication are 2.6×10^{-4} S cm^{-1} and 5.3×10^{-7} S cm^{-1} respectively at room temperature.

The cell of configuration Lithium Transition metal/Polymer/ MS where M = Pb or Sn were fabricated and is shown schematically below.

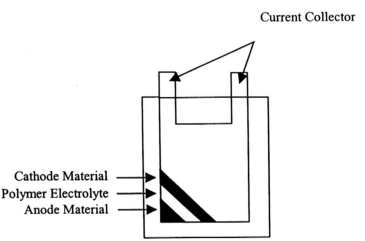

Figure 4.23. A schematic representation of the fabricated cell.

4.7.2 Charge / discharge Characteristics

In this section the characteristics of the fabricated batteries will be presented.

(i) Li transition metal / polymer/PbS (C1)

The charging and discharging profile of this fabricated cell is depicted in Figure 4.24. The cell was then charged at 50 mA for 1 hour and discharge at 1.0 mA for 15 hours. The expected capacity of the cell on completion of charge is 50 mAh. Since the cell was discharged at 1mA for 15 hours this indicated that it already spent 15 mA h after 15 hours. At this rate, capacity of the cell is 35 mA h. Therefore the battery is expected to last for another 35 hours. The discharge characteristic of the battery shows that it takes 16 hours for the voltage to drop from 2.4 V to 1.0 V when discharged under a load current 1.0 mA. The voltage depletion is thought to be caused by the interfacial resistance between the anode - electrolyte and cathode - electrolyte interface.

(ii) Li transition metal / polymer / SnS (C2)

The battery was charged at 50 mA for 2 hours and discharge at 1.0 mA for 7 hours. The cell is expected to have a capacity of 100 mA h. During the first cycle the cell was charged up to 2.9 V and upon discharge the voltage dropped to one 0.6 V. The observation is shown in Figure 4.25. Again the drop in voltage could be attributed to the electrode - electrolyte contact problem.

In this study, the battery system investigated is of the configuration

Li Transition Metal Oxide / polymer / MS

where M = Pb or Sn. This cell makes use of a lithium transition metal oxide as the cathode, a chitosan based polymer as the electrolyte and the metal sulphides (MS) as the anode . The analysis of the cells will be described in this work. A schematic representation of the fabricated cell is shown in Figure 4.23.

A satisfactory charging curve was obtained implying that the lithium ion in the lithium transition metal have been successfully inserted to the anode i.e charge has been transferred into the anode. However the performance of the cell must still be improved since there is a voltage drop for the PbS cell and for the SnS cell on discharge.

The discharge characteristic of the cell with PbS as anode shows that it takes 16 hours for the voltage to drop from 2.4 V to 1.0 V when discharged under a load current of 1.0 mA while for SnS the voltage drop from 2.8 V to 0.6 V within 9 hours under a load current of 1.0 mA. This phenomenon is probably due to increase in cell resistance.

Another possible explanation for the large drop in voltage upon discharge for both anode materials could be due to the formation of Solid Electrolyte

Interphase (SEI) on the surface of the alloy anode which was observed when amorphous Sn-Ca alloy was used as anode for lithium ion cell (Fang and Chowdari, 2000).

Solid Electrolyte Interphase is the formation of the layer occurring at the electrolyte/anode (electrode) interface. This layer makes a potential barrier to the electrons and thus the tunneling of electrons through layer is stopped. However SEI layer allows ionic transfer from the electrolyte side to the electrode thus assuring the continuation of the electrochemical operation.

The voltage drop in the second cycle for both anodes is probably due to the formation of multphases (Li_xSn or Li_xPb). The formation of the multiphases increased internal resistance thus causing battery failing to work. Other factors are attributed to polarization and humidity.

In a more recent report it was noted that surface cleanliness and uniformity of high conductivity are the two most important key factors for attaining high power and long cycle life (Suzuki et al., 2000).

These preliminary results indicate that both PbS and SnS can insert and deinsert lithium ion and thus has the potential to act as anode material in

lithium ion cells. The results also indicate SnS is less efficient than PbS as anode for Li ion cell. This could be due to the different methods of synthesis and the electrical conductivity of PbS is higher than SnS.

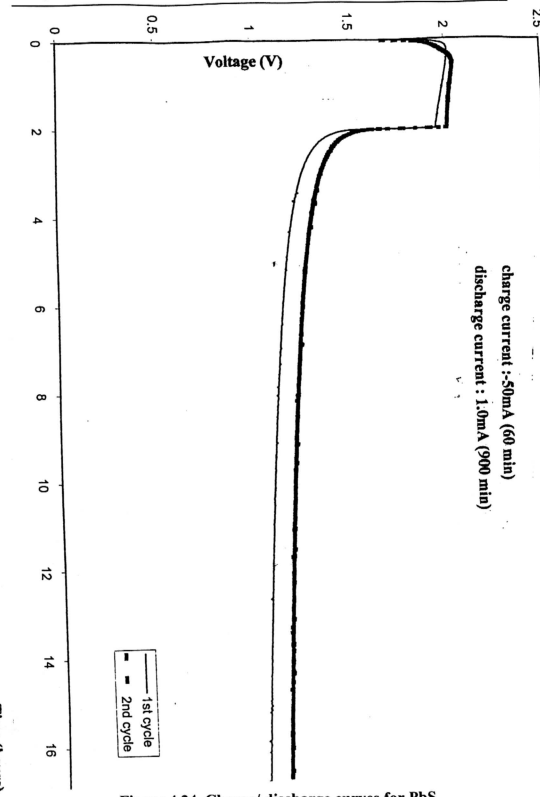

Figure 4.24. Charge/ discharge curves for PbS.

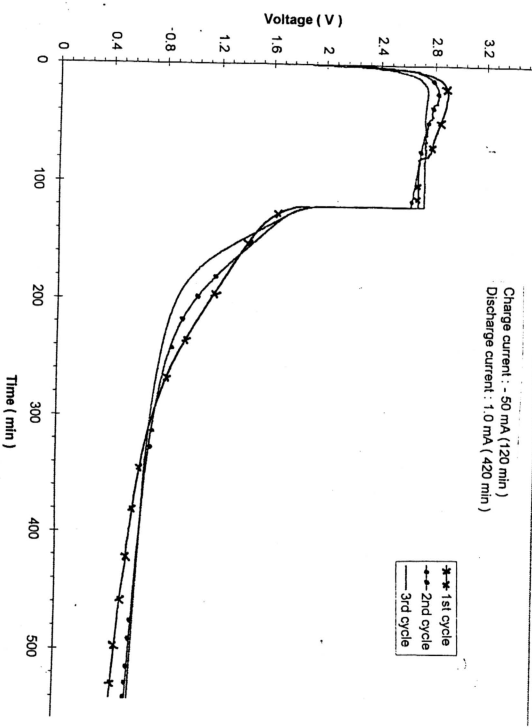

Figure 4,25. Charge / discharge curves for SnS.